# Photochemistry of 2-butenedial and 4-oxo-2-pentenal under atmospheric boundary layer conditions

**Mike J. Newland[1], Gerard J. Rea[2], Lars P. Thüner[2], Alistair P. Henderson[3], Bernard T. Golding[3], Andrew R. Rickard[1,4], Ian Barnes[5,**], John Wenger[2]**

[1] *Wolfson Atmospheric Chemistry Laboratories, Department of Chemistry, University of York, UK*
[2] *School of Chemistry and Environmental Research Institute, University College Cork, Cork, Ireland*
[3] *School of Natural and Environmental Sciences, Bedson Building, Newcastle University, Newcastle upon Tyne, UK*
[4] *National Centre for Atmospheric Science, Wolfson Atmospheric Chemistry Laboratories, University of York, UK*
[5] *University of Wuppertal, School of Mathematics and Natural Science, Institute of Atmospheric and Environmental Research, Wuppertal, Germany*
[**] *deceased*

## Abstract

Unsaturated 1,4-dicarbonyl compounds, such as 2-butenedial and 4-oxo-2-pentenal are produced in the atmospheric boundary layer from the oxidation of aromatic compounds and furans. These species are expected to undergo rapid photochemical processing, affecting atmospheric composition. In this study, the photochemistry of (*E*)-2-butenedial and both *E* and *Z* isomers of 4-oxo-2-pentenal was investigated under natural sunlight conditions at the large outdoor atmospheric simulation chamber EUPHORE. Photochemical loss rates, relative to $j(NO_2)$, are determined to be $j((E)\text{-2-butenedial})/j(NO_2) = 0.14$ (±0.02), $j((E)\text{-4-oxo-2-pentenal})/j(NO_2) = 0.18$ (±0.01), and $j((Z)\text{-4-oxo-2-pentenal})/j(NO_2) = 0.20$ (±0.03). The major products detected for both species are a furanone (30 – 42%) and, for (*E*)-2-butenedial, maleic anhydride (2,5-furandione) (12 – 14%). The mechanism appears to proceed predominantly *via* photoisomerization to a ketene-enol species following γ-H abstraction. The lifetimes of the ketene-enol species in the dark from 2-butenedial and 4-oxo-2-pentenal are determined to be 465 s and 235 s, respectively. The ketene-enol can undergo ring closure to yield the corresponding furanone, or further unimolecular rearrangement which can subsequently form maleic anhydride. A minor channel (10 – 15%) also appears to form CO directly. This is presumed to be *via* a molecular elimination route of an initial biradical intermediate formed in photolysis, with an unsaturated carbonyl (detected here but not quantified) as co-product. α-dicarbonyl and radical yields are very low, which has implications for ozone production from the photo-oxidation of unsaturated 1,4-dicarbonyls in the boundary layer. Photochemical removal is determined to be the major loss process for these species in the boundary layer with lifetimes of the order of 10 – 15 minutes, compared to > 3 hours for reaction with OH.

## Introduction

Unsaturated 1,4-dicarbonyl compounds, such as 2-butenedial and 4-oxo-2-pentenal (Figure 1), are expected to be ubiquitous in the atmospheric boundary layer. They have both anthropogenic and natural sources including: oxidation of aromatic compounds (e.g. benzene, toluene, xylenes)[1], emitted from solvents and fossil fuel combustion; and oxidation of furans[2-4], produced in large quantities from biomass burning and currently being developed as second-generation biofuels[5]. It is generally accepted that unsaturated 1,4-dicarbonyls are major products from ring opening of the peroxide bicyclic species produced in OH addition reactions with aromatic compounds[6-9], although the importance of this route has recently been questioned[10,11]. Unsaturated 1,4-dicarbonyls have been detected in the oxidation of benzene[1,12], toluene[1,13-15], xylenes, and the trimethyl benzenes[14,16].


**Figure 1** Structures of (*E*)-2-butenedial and (*Z*)-4-oxo-2-pentenal.

There have been relatively few studies to date on the oxidation pathways and products, and hence their effect on atmospheric chemistry and ozone formation, of these important intermediate species. This is in part due to their unstable and highly reactive nature, meaning that they are not commercially available and must be synthesized. Furthermore, they are difficult to analyse using chromatographic methods, owing to their polar nature and co-elution with other products[13,16,17]. However, derivatisation techniques have been used with some success to identify butenedial and 4-oxo-2-pentenal from retention time and mass spectral comparisons with synthesized standards[13,16-18].

Photochemical removal is thought to be the major fate of unsaturated 1,4-dicarbonyls in the atmosphere, with previously reported loss rates of 2-butenedial and 4-oxo-2-pentenal on the order of $0.8 - 2 \times 10^{-3}$ $s^{-1}$ [19], giving a lifetime with respect to photochemical removal of ~ 10 - 20 minutes. Reaction with OH for these compounds is of the order of $2 – 6 \times 10^{-11}$ $cm^{-3}$ $s^{-1}$ [19] giving a lifetime of 3 – 7 hours at $[OH] = 2 \times 10^6$ $cm^{-3}$. These rates are structure dependent, with Bierbach *et al.*[19] determining both the

photochemical loss rate and OH reaction rate of (*Z*)-2-butenedial to be about a factor of two greater than for (*E*)-2-butenedial.

Previous chamber studies[6,19] have reported the major products of 1,4-dicarbonyl photochemistry to be 2(3*H*)-furanone (from 2-butenedial), 5-methyl-2(3*H*)-furanone (from 4-oxo-2-pentenal), and maleic anhydride. On the other hand, flow tube laser photolysis studies at 308 and 351 nm determined the furanones to be minor products: quantum yield < 2% for 2-butenedial[20] and ~ 5% for 4-oxo-2-pentenal[21]. No maleic anhydride was detected in these studies as they were performed in the absence of oxygen. Formyl radical (HCO) production was also found to be negligible at atmospherically relevant wavelengths of 308 and 351 nm, indicating that photodissociation of the parent compound is unlikely to be important for radical production under boundary layer conditions. The major end products observed at wavelengths relevant to the troposphere in these flow tube studies were acrolein (from 2-butenedial – ≥15% and ≥23% at 308 nm and 351 nm respectively) and methyl vinyl ketone (from 4-oxo-2-pentenal – 40% and 33% at 308 nm and 351 nm respectively). Liu *et al.*[22] also detected these unsaturated carbonyls in very small amounts during the photo-oxidation of 2-butenedial and 4-oxo-pentenal in a chamber; the instrumentation used in this case was not capable of measuring furanones or maleic anhydride.

Photolysis of short chain saturated *n*-aldehydes, at wavelengths relevant to the boundary layer (i.e. > 290 nm), occurs mainly via α-cleavage of the carbon-carbon bond *i.e.* Norrish Type I reaction[23] (Figure 2). This reaction generates two radicals. For longer chained aldehydes (≥ C4), Norrish Type II photolysis has been observed to become increasingly important[24,25]. The standard Norrish Type II process for saturated aldehydes involves intramolecular γ-H atom abstraction (hence cannot occur for aldehydes with a smaller carbon chain than *n*-butanal and for branched aldehydes where a γ-hydrogen is not available), leading to a 1,4-biradical (Figure 2). This species can either fragment to yield an alkene and an enol, or cyclise to form a cyclobutanol[26]. The enol formed in 2-pentanone photolysis (2-propenol) has been observed in laboratory experiments to isomerize to acetone on a timescale of minutes[27,28]. A small activation energy of ~ 2 kcal $mol^{-1}$ was determined for this process, the authors concluded that the conversion is most likely driven by the reactor walls. Shaw *et al.*[28] also investigated the photolysis of 2-methylbutanal, leading to the enol 1-propenol, and found the tautomerization of 1-propenol to propanal to be considerably slower than that of 2-propenol to acetone.

There has been little work on the photochemistry of unsaturated carbonyls. Coomber *et al.*[29] investigated the photochemistry of (*E*)-2-butenal (*E*-crotonaldehyde) and detected products presumed to be ethylketene and 1,3-butadienol, i.e. the enol and unsaturated hydrocarbon products expected from a Norrish Type II type process (where the unsaturated hydrocarbon retains the carbonyl group forming a ketene). O'Connor *et al.*[30] studied the photochemistry of three unsaturated $C_6$ aldehydes using natural

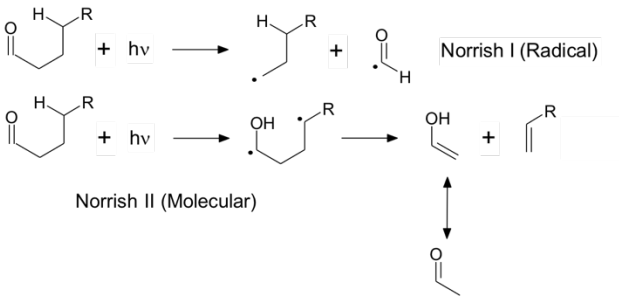


**Figure 2** Norrish Type I and Norrish Type II photolysis processes.

sunlight. (*E*)-2-Hexenal and (*E*,*E*)-2,4-hexadienal were found to undergo rapid isomerization to produce (*Z*)-2-hexenal and a ketene-type compound (probably (*E*)-hexa-1,3-dien-1-one), respectively. Atmospheric photolysis of (*Z*)-3-hexenal proceeded via a Norrish type I process producing 2-pentenal and CO.

This work describes the first detailed experiments on the photochemistry of *(E)*-2-butenedial, *(Z)*-4-oxo-2-pentenal and *(E)*-4-oxo-2-pentenal under ambient light conditions. Experiments were performed at the European Photoreactor (EUPHORE) in October 2001 and July 2002 as part of the EXACT campaign[6]. A detailed analysis of these experiments is performed here to improve the mechanistic understanding of the photochemistry of unsaturated 1,4-dicarbonyls in the atmosphere, relevant for implementation in air quality and climate models (e.g. the Master Chemical Mechanism (MCM)[31]).

## Experimental

The photochemistry of (*E*)-2-butenedial, (*Z*)-4-oxo-2-pentenal and (*E*)-4-oxo-2-pentenal was investigated in the outdoor European Photoreactor EUPHORE in Valencia, Spain (39º 30′ N, 0º 30′ W). EUPHORE has two hemispherical reaction chambers (volume of ca. 200 $m^3$) made of highly transparent FEP Teflon (polyfluoroethene propene copolymer), which assures an even distribution of natural sunlight inside. The reaction chambers have protective housing which can be opened and closed automatically within two minutes. This allows experiments to also be performed in the dark, with the measured photolysis rate of $NO_2$ ($j(NO_2)$) < $10^{-6}$ $s^{-1}$ when the housing is closed. Two fans inside the chambers allow for rapid homogeneous mixing. Experiments were performed in dry purified air, which is scrubbed of non-methane hydrocarbons, $NO_x$ and particles. Further details of the chamber setup and instrumentation are available elsewhere[32,33].

(*E*)-2-butenedial, (*Z*)-4-oxo-2-pentenal, (*E*)-4-oxo-2-pentenal, 2(3*H*)-furanone and 5-methyl-2(5*H*)-furanone are not commercially available and were synthesized using methods based on those reported in the literature. Details of the syntheses are provided in the Supplementary Information. The relative complexity of the syntheses and the instability of the dicarbonyls limited the amounts available. The reaction products 2(3*H*)-furanone and 5-methyl-2(5*H*)-furanone were synthesized to provide reference FTIR spectra. All synthesized samples were estimated to

be > 90% purity, from interpretation of their NMR spectra, with the exception of 2(3*H*)-furanone which was estimated to have a 21% impurity of 2(5*H*)-furanone based on its gas-phase FTIR spectrum. 5-methyl-2(3*H*)-furanone and 2(5*H*)-furanone were purchased from Aldrich with a reported 98% purity.

All experiments were performed in the temperature range 297 - 303 K. For each experiment the temperature did not change more than 1.2 K during the short experiments (30 – 60 minutes) and not more than 3.6 K during longer interval experiments. The light intensity and spectral distribution was measured inside the chamber using a spectroradiometer (Bentham TM300) with a time resolution of 8 min. Photochemical loss rates *e.g.* $j(NO_2)$ were calculated from these data using the appropriate cross-section and quantum yield values[34]. Comparison of $j(NO_2)$ values calculated from the spectroradiometer data with those obtained by an independently calibrated $j(NO_2)$ filter radiometer showed that values from the two instruments were within 10% of each other. The uncertainty in measurement of the absolute light intensity was thus less than 10%. Quantification of precursor reactants and products was performed using *in situ* long-path FTIR spectroscopy, with a 53.5 m optical path length in the range of 4000 - 650 $cm^{-1}$ and 1 $cm^{-1}$ resolution (Nicolet Magna 550, liquid $N_2$ cooled MCT detector). Spectra were taken by co-adding 50, 110 or 225 interferograms, which resulted in a time resolution of 1, 2 or 4 minutes respectively. Concentrations were determined by computer aided subtraction of calibrated reference spectra of authenticated standards. During the experiments 63 – 95% of the initial reactant was consumed within the experimental duration, which ranged from 25 – 90 minutes.

2-Butenedial and 4-oxo-2-pentenal are very sensitive to light and heat. Therefore, they were injected into the dark reaction chamber using one of two approaches; either dissolved in 0.5 - 1 ml of HPLC grade acetonitrile and then sprayed into the chamber in a high-pressure stream of purified air or slightly warmed while neat and allowed to enter the chamber through a stream of purified air. Reaction of acetonitrile with the aldehydes was not observed in the solution or in the chamber. Inert $SF_6$ (~ 25 ppbv) was typically added to the reaction mixture as a tracer of the dilution owing to chamber leakage and sampling losses. In all experiments the dilution loss was determined to be ~ 1% over the duration of the experiments and therefore no corrections for dilution of reactant and products were applied.

**Table 1** Initial conditions of EUPHORE photochemistry experiments [a]. EBUT: (*E*)-2-butenedial; ZOXO: (*Z*)-4-oxo-2-pentenal; EOXO: (*E*)-4-oxo-2-pentenal.

| Date | Experiment ID | Initial Carbonyl Conc. (ppbv) | Comments |
|---|---|---|---|
| 01 Oct 01 | EBUT01 [b] | 90 | ~ 1 ppmv *iso*-propanol added as OH scavenger |
| 01 Oct 01 | EBUT02 [b] | 438 | |
| 02 Oct 01 | ZOXO01 [b] | 464 | |
| 03 Oct 01 | ZOXO02 [b] | 343 | |
| 04 Oct 01 | EBUT03 [b] | 549 | Chamber opened and closed multiple times to investigate formation of ketene |
| 05 Oct 01 | ZOXO03 [b] | 540 | |
| 15 Jul 02 | EOXO01 [b] | 200 | ~ 1 ppmv *iso*-propanol added as OH scavenger |
| 15 Jul 02 | EOXO02 [b] | 168 | |
| 16 Jul 02 | EBUT04 [c] | 256 | No added OH scavenger |
| 16 Jul 02 | EBUT05 [c] | 243 | |
| 17 Jul 02 | ZOXO04 [c] | 319 | |
| 17 Jul 02 | ZOXO05 [c] | 220 | |

[a] Chamber temperature during experiments 297 – 303 K.
[b] Reactant sprayed into chamber in solution of acetonitrile
[c] Reactant addition performed in a stream of gently heated purified air

As the sample of (*E*)-4-oxo-2-pentenal used during this study contained unidentified impurities it was not possible to directly determine the starting concentration of reactant in the experiments. However, this information was derived from a simulation of the concentration-time profiles for photolysis of both (*E*)-and (*Z*)-isomers of 4-oxo-2-pentenal. The simulations rely on the fact that the observed ketene intermediate is the same for both 4-oxo-2-pentenal isomers. First of all, a spectral response factor was obtained for the ketene intermediate by simulating the concentration-time data in experiment ZOXO02 (Table 1). The response factor for the ketene was subsequently used in a simulation of the concentration-time data obtained in experiments EOXO01 and EOXO02 to estimate response factors for (*E*)-4-oxo-2-pentenal of 189 and 195 respectively. An average response factor of 192 was therefore used to determine an estimate of the initial concentration of (*E*)-4-oxo-2-pentenal in the experiments.

The photochemistry of (*E*)-2-butenedial and (*Z*)-4-oxo-2-pentenal was investigated in the presence and absence of an OH radical scavenger (*iso*-propanol (~ 1000 ppbv)). The photochemistry of (*E*)-4-oxo-2-pentenal was investigated only in the presence of the OH radical scavenger. Initial experimental conditions are given in Table 1.

## Results and Discussion

### Photochemical loss rates

The first order loss rates for the unsaturated 1,4-dicarbonyls were determined in each experiment. The concentration-time data for the reactant loss was treated using Equation E1:

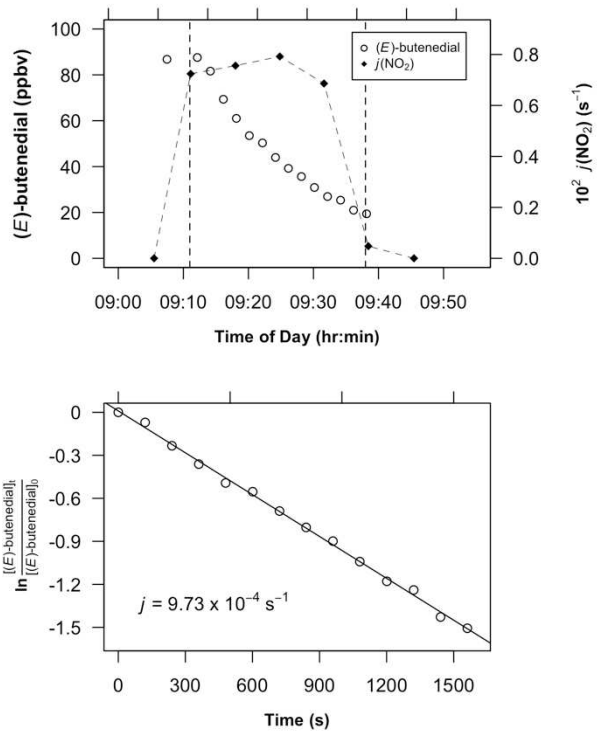


**Figure 3** Top: Concentration time profile of *(E)*-2-butenedial (ppbv) and $j(NO_2)$ ($s^{-1}$) from experiment EBUT01. Bottom: Linear regression of loss rate of *(E)*-2-butenedial in EBUT01.

$$\ln \frac{[A]_t}{[A]_0} = -jt \qquad \text{(E1)}$$

An example concentration-time profile and corresponding first order rate plot for an *(E)*-2-butenedial experiment (EBUT01) is shown in Figure 3. Linear regression analysis of the plots enabled determination of the slope of the straight line and thus the photochemical loss rate coefficient, *j*. The associated $j(NO_2)$ values measured in the chamber are also plotted, and used to calculate *j*(dicarbonyl)/$j(NO_2)$ values for each experiment. This enables direct comparison of the photochemical loss of the unsaturated 1,4-dicarbonyls under different ambient sunlight conditions. The determined rates are summarised in Table 2. In some cases, when $j(NO_2)$ could not be measured directly, the value determined in the adjacent chamber (identical in design) was used.

**Table 2** Summary of observed photochemical loss rates [a].

| Experiment | $10^4$ *j*(dicarb.) ($s^{-1}$) | $10^3$ *j*($NO_2$) ($s^{-1}$) | *j*(dicarb.)/ *j*($NO_2$) |
|---|---|---|---|
| EBUT01 | 9.7 | 7.4 | 0.13 (± 0.02) |
| EBUT02 | 1.6 – 5.4 | 1.0-2.8 | 0.15 (± 0.02)[b] |
| EBUT04 | 12.4 | 8.8 | 0.14 (± 0.01) |
| EBUT05 | 9.5 | [c] | [c] |
| ZOXO01 | 16.5 | 9.1 | 0.18 (± 0.01) |
| ZOXO02 | 15.2 | 6.9 | 0.22 (± 0.02) |
| ZOXO04 | 16.4 | 8.2 | 0.20 (± 0.02) |
| ZOXO05 | 16.0 | 7.8 | 0.19 (± 0.04) |
| EOXO01 | 13.7 | 7.3 | 0.19 (± 0.01) |
| EOXO02 | 13.0 | 7.5 | 0.17 (± 0.01) |

[a] Except for $j(NO_2)$, quoted errors are twice the standard deviation arising from the least squares fit of the data and include the uncertainty in calibration and response factors. For $j(NO_2)$, and the maximum theoretical loss rate, the estimated error is 10%.
[b] Determined from overlapping three point averages
[c] No $j(NO_2)$ data available

The mean *j*(dicarbonyl)/$j(NO_2)$ values from all the experiments for the three unsaturated 1,4 dicarbonyls are: *j((E)*-2-butenedial)/$j(NO_2)$ = 0.14 (± 0.02), *j((E)*-4-oxo-2-pentenal)/$j(NO_2)$ = 0.18 (± 0.01), and *j((Z)*-4-oxo-2-pentenal)/$j(NO_2)$ = 0.20 (± 0.03).

These rates are ~ 20% higher than those determined by Bierbach *et al.*[19] in indoor chamber experiments using UV-visible lamps ($320 \le \lambda \le 480$ nm, $\lambda_{max} = 360$ nm). Assuming a noontime value for $j(NO_2)$ of $8 \times 10^{-3}$ $s^{-1}$ they calculated rates of $0.9 \times 10^{-3}$ $s^{-1}$ for *(E)*-2-butenedial and $1.3 \times 10^{-3}$ $s^{-1}$ for a mixture of *(E)*- and *(Z)*-4-oxo-2-pentenal. In flow tube laser photolysis studies, Xiang *et al.*[21] calculated absorption cross sections at atmospherically relevant wavelengths between 190 and 460 nm for *(E)*- and *(Z)*-4-oxo-2-pentenal. They determined removal rates for *(Z)*-4-oxo-2-pentenal of $0.88 \times 10^{-3}$ $s^{-1}$ – $0.55 \times 10^{-3}$ $s^{-1}$ and for *(E)*-4-oxo-2-pentenal of $0.69 \times 10^{-3}$ $s^{-1}$ – $0.41 \times 10^{-3}$ $s^{-1}$. This rate for *(Z)*-4-oxo-2-pentenal is roughly a factor of two lower than determined in the current study.

The presence of an OH scavenger has no obvious effect on the observed loss rates for the unsaturated 1,4 dicarbonyls (Table 2), suggesting that even in experiments without an OH scavenger, reaction with OH remains a minor sink compared to photochemical removal. In experiments EBUT05, ZOXO04 and ZOXO05, all of which had no OH scavenger, OH was measured by laser induced fluorescence[35] to be ~ $4 – 6 \times 10^6$ $cm^{-3}$ for the duration of the experiment (Figure S6). Using a representative value of $k_{OH}$(dicarbonyl) ~ $4 \times 10^{-11}$ $cm^3$ $s^{-1}$ [19], gives an OH reaction loss rate of ~ $2 \times 10^{-4}$ $s^{-1}$ in these experiments, indicating that OH reaction should thus account for *ca.* 15% of the total loss in EBUT05 and *ca.* 11 % in ZOXO05 and ZOXO06. The fact that the loss rates of the parent compounds appear relatively unaffected in the presence and absence of OH scavenger suggests that the OH + 1,4-unsaturated dicarbonyl reaction rates may be slower than previously reported[19]. However, it is also noted that the LIF OH detection limit in the chamber is ~ $1 \times 10^6$ $cm^{-3}$, with an overall uncertainty of ~ 25 % on the OH calibration[36].

Comparison of the relative *j*-values in Table 2 shows that the (*Z*)- isomer of 4-oxo-2-pentenal is more readily lost than the (*E*)-isomer. Comparing the mean relative *j*-value of 0.14 (± 0.02) for *(E)*-2-butenedial from Table 2 with the relative *j*-value for (*Z*)-2-butenedial of 0.18 (± 0.01) from work by Sørenson and Barnes[37], also performed in the EUPHORE chamber, shows the same relationship for these isomers. This relationship may be explained by the observed formation of a ketene intermediate during photochemical processing (Figure 4). This ketene intermediate is presumed to form by photoexcitation followed by intramolecular rearrangement *via* a γ-H abstraction process. The γ-H shift is only possible for the (*Z*)-isomer of each compound, as the (*E*)-isomer cannot form the required six-membered transition state. Thus, while the (*Z*)-isomers are initially in the ideal form for conversion to the ketene, the (*E*)-isomers need to undergo isomerization

prior to γ-H abstraction. There is no evidence for isomerization from the *(E)*- to the *(Z)*-isomer in the FTIR spectra and therefore it is possible that the (*E*)-isomer may be photoexcited and then undergoes subsequent isomerization directly to produce the configuration required for intramolecular rearrangement. This will provide an extra energy barrier for the reaction and thus results in lower *j*-values than for the corresponding (*Z*)-isomers.

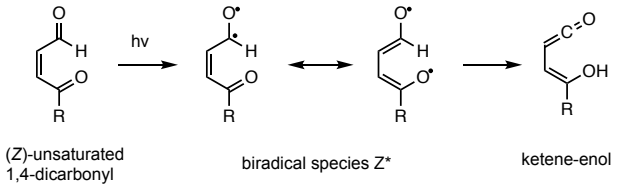


**Figure 4** Formation of ketene-enol species via Norrish Type II photoisomerization of a (*Z*)-unsaturated 1,4-dicarbonyl. (R=H, 2-butenedial; R=$CH_3$, 4-oxo-2-pentenal).

The *j*-values presented in Table 2 also show that 4-oxo-2-pentenal is more readily photochemically removed than 2-butenedial. The reverse behaviour may be expected, as molecules containing the aldehyde functional group are more susceptible to photolysis by sunlight than those containing the ketone functional group. The aldehyde functional group is the principal chromophore and $\pi^* \leftarrow n$ excitation preferentially takes place in this part of the dicarbonyls to initially produce a photoexcited complex in the form of a biradical species (Z* in Figure 4). The conjugated nature of the system facilitates delocalization of electron density throughout the $\pi$ orbitals. As the electronic charge is shared throughout the conjugated system, added substituents act to further stabilize the radical. The photoexcited complex for 4-oxo-2-pentenal (Z*) is a secondary radical (because of the methyl substituent) and is therefore an intrinsically more stable species than the primary radical formed from photoexcitation of 2-butenedial. Thus the formation of the 4-oxo-2-pentenal photoexcited complex is more favourable, and hence photoisomerization will proceed more rapidly.

Table S1 (Supplementary Information) provides a comparison of photochemical loss rates of other saturated and unsaturated aldehydes determined from studies at EUPHORE. The photochemical loss rates of the unsaturated 1,4-dicarbonyls measured here are roughly two orders of magnitude faster than those of saturated aldehydes. For example, for n-hexanal, a *j*-value of $1.8 \times 10^{-5}$ $s^{-1}$ is calculated for $j(NO_2) = 9 \times 10^{-3}$ $s^{-1}$ [38,39].

For the unsaturated but non-conjugated species (*Z*)-3-hexenal, a very similar rate to n-hexanal is calculated; whereas for the conjugated isomer, (*E*)-2-hexenal, the calculated *j*-value is approximately four times higher[30]. The *j*-values reported for the fully conjugated dienal species, 2,4-hexadienedial, are another order of magnitude higher again[40], and similar to those of 2-butenedial and 4-oxo-2-pentenal. Clearly, the effect of increasing conjugation is to greatly enhance the rate of photolysis under sunlight. However, it should be emphasized that the main pathway for the photochemical loss of the conjugated C6 aldehydes is isomerization rather than photodissociation[30,40].

## Products

Products were identified and quantified using *in situ* FTIR spectroscopy. A typical series of spectra obtained for an (*E*)-2-butenedial experiment is shown in Figure 5. The major identified products of (*E*)-butenedial photochemistry were 2(3*H*)-furanone, maleic anhydride (2,5-furandione) and CO. During the reaction, a ketene compound was observed with a characteristic absorption in the C=C=O stretching region at 2138 $cm^{-1}$ [41]. A carbonyl compound with a C=O stretching absorption band around 1819 $cm^{-1}$ was also observed as a major product but could not be identified from available spectra. Other compounds identified as minor reaction products include formaldehyde, glyoxal, methylglyoxal, 2(5*H*)-furanone and acrolein. For the 4-oxo-2-pentenal isomers, the major identified products were 5-methyl-2(3*H*)-furanone and CO. As in the 2-butenedial system, a ketene intermediate was also observed (C=C=O stretch at 2135 $cm^{-1}$), and a C=O absorption at approximately 1829 $cm^{-1}$ remained in the residual spectra after subtraction of all known compounds. Other compounds identified as minor reaction products were maleic anhydride, formaldehyde, glyoxal, methylglyoxal, acrolein and methyl vinyl ketone. Many of these minor products have been identified in earlier photo-oxidation studies of unsaturated 1,4 dicarbonyls[19-22].

Concentration-time profiles of reactant and products were generated for each experiment by spectral subtraction of calibrated reference spectra. The concentration of the unidentified carbonyl in each of the reaction systems was estimated by using the absorbance of the carbonyl peak at 1811 $cm^{-1}$ in the reference spectrum of 2(5*H*)-furanone.

**Table 3** Yields (%) of major products with respect to the parent dicarbonyl observed in photochemistry experiments with and without OH scavenger [a]

| Product | (*E*)-2-butenedial | | (*Z*)-4-oxo-2-pentenal | | (*E*)-4-oxo-2-pentenal |
|---|---|---|---|---|---|
| | OH scav. | No OH scav. | OH scav. | No OH scav. | OH scav. |
| 2(3*H*)-furanone [b] | 41 (± 5) | 41 (± 1) | | | |
| 5-Methyl-2(3*H*)-furanone | | | 30 (± 2) | 42 (± 1) | 32 (± 3) |
| Maleic Anhydride | 14 (± 2) | 12 (± 2) | 3 (± 0.5) | 4 (± 0.5) | 6 (± 0.5) |
| Primary CO [c] | 20 (± 2) | 18 (± 3) | 10 (± 1.5) | 13 (± 2) | 15 (± 5) |
| Unknown carbonyl (1819 $cm^{-1}$) | 9 (± 2) | 7 (± 1) | | | |
| Unknown carbonyl (1829 $cm^{-1}$) | | | 16 (± 1.0) | 20 (± 2) | 24 (± 7) |

[a] Quoted errors include the uncertainty in calibration and response factors, and the fit to the data. [b] 2(5*H*)-furanone also measured with yield of ~ 10 % of 2(3*H*)-furanone [c] determined from CO yield during early part of experiment, while yield is linear.

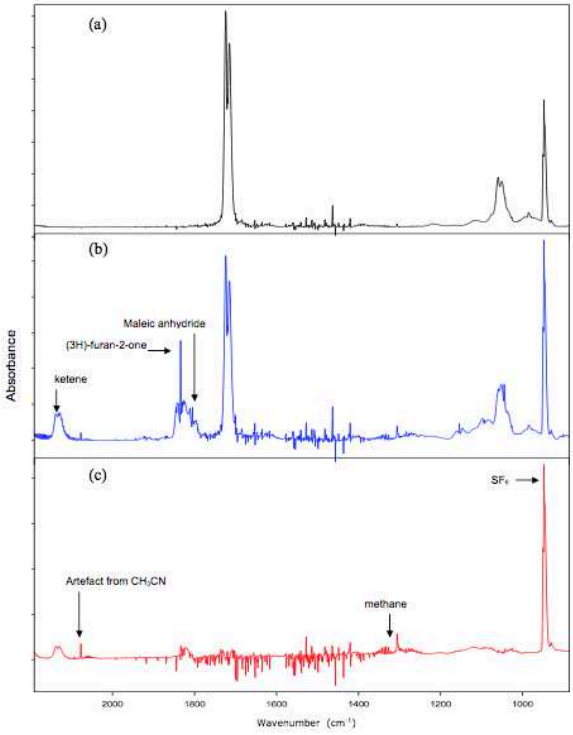


**Figure 5** FTIR spectra obtained for (*E*)-2-butenedial, experiment EBUT02: (a) before exposure to sunlight; (b) during exposure; (c) residual obtained following subtraction of all known products.

There were no reference spectra available for the ketene intermediates formed in the experiments and the change in peak height of the characteristic absorption in the C=C=O stretching region was used to follow the temporal evolution of these species. Response factors of the ketene were determined by constraining to the loss rates derived from the measured concentrations of the parent compound, and assuming loss rates of the ketene as determined from measurements of the ketene lifetime in the dark (Table 4). An estimated yield of 0.8 for the ketene from *(E)*-2-butenedial and 0.9 for the ketene from 4-oxo-2-pentenal was based on the measured CO yield (assumed not to come from the ketene) in the early stages of the experiments. The measured absorbances were then multiplied by the response factors to give the corresponding volume mixing ratios in ppbv.

An example concentration-time plot for *(E)*-2-butenedial (experiment EBUT05) is presented in Figure 6. The rapid loss of the unsaturated 1,4-dicarbonyl (top panel) yields the ketene intermediate. This decays to give a number of products (bottom panel). The yield of CO in the early part of the experiments appears to be linear (Figure 7), indicating that CO is likely a primary product of photolysis. The yield appears to increase with time during most of the experiments, suggesting that there are also secondary sources of CO. In contrast, the concentration-time profiles of the cyclic reaction products, the furanone and maleic anhydride, are non-linear, indicating that they are secondary products, presumed to be generated from the decay of the ketene intermediate.

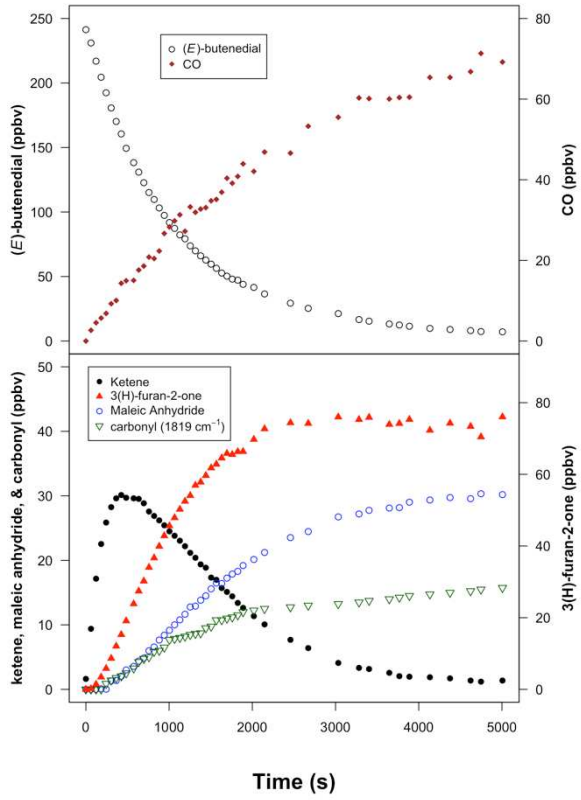


**Figure 6** Time series of major products (ppbv) detected in (*E*)-2-butenedial experiment EBUT05. Top panel: (*E*)-2-butenedial decay and CO formation. Bottom panel: Ketene intermediate and major products derived from its subsequent chemistry. (Ketene response factor determined to be 853.45 using method described in text).

Table 3 provides a summary of the yields of the major products with respect to the parent dicarbonyls detected during the experiments. Since a number of the products appear not to be primary photochemical products, yields are shown in Figure 8 (and Supp. Info. Figure S7-S9) as the loss of the reactant against product. For CO, the reactant in the initial stages of the experiment is assumed to be the parent compound. For the furanone and the unidentified carbonyl, the reactant is assumed to be the ketene-enol. Production and loss of the ketene-enol was determined from model simulations (described below). For maleic anhydride, the reactant is assumed to be a ketene-carbonyl, the tautomer of the ketene-enol.

A number of experiments were performed to further investigate the chemical reactivity of the ketene intermediates formed in each of the unsaturated dicarbonyl systems, and their relationship to the final observed products. In these experiments, the chamber was partially opened for 5-25 min and then closed for a similar amount of time. This sequence was repeated several times until most of the dicarbonyl was consumed (Figure S10 & S11 – Supp. Info). The same general pattern was observed during experiments for both (*E*)-2-butenedial and (*Z*)-4-oxo-2-pentenal: immediately after the chamber was opened, there was a rapid decay of the dicarbonyl and an equally rapid formation of the ketene intermediate.

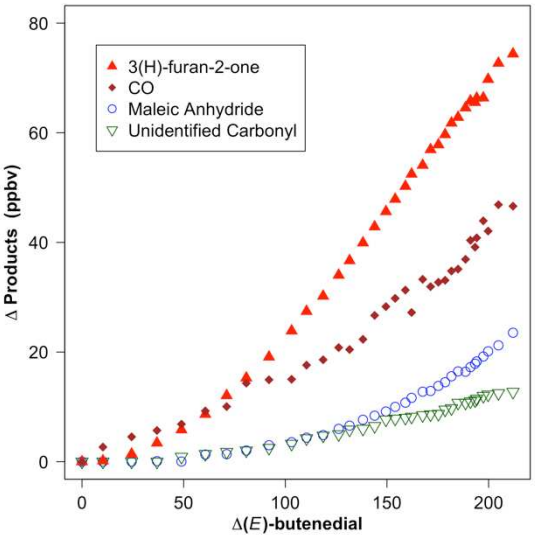


**Figure 7** Measured mixing ratios (ppbv) of major products of (*E*)-2-butenedial photochemistry against loss of (*E*)-2-butenedial for experiment EBUT05.

During the first "open chamber" period there was virtually no formation of the major cyclic reaction products. As soon as the chamber was closed, the decay of the dicarbonyl stopped and a dramatic drop in ketene concentration was observed. The subsequent increase in concentration of the cyclic reaction products whilst the chamber was closed indicates that they originate from the decomposition of the ketene in the dark, rather than from direct photodissociation of the dicarbonyl. When the ketene concentration was stable, the chamber was reopened and closed again and the reaction sequence was repeated. At the end of the experiments virtually no ketene remained.

Table 4 shows the first order loss rates and corresponding lifetimes for the ketenes in the dark. These were determined from experiments in which the chamber housing was closed after removal of 50 – 80 % of the initial parent compounds (e.g. Figures S12 – S13). Photochemical production of the ketene stops when the chamber is closed. The loss rate of the ketene can then be determined. The mean loss rate for the ketene in the dark during the (*E*)-2-butenedial experiments is $2.15 \times 10^{-3}$ $s^{-1}$, while for the ketene from the 4-oxo-2-pentenal experiments it is $4.25 \times 10^{-3}$ $s^{-1}$. The good agreement between the values for (*E*) and *(Z)*-4-oxo-2-pentenal is consistent with these two isomeric compounds producing the same ketene species.

## Photochemical Mechanism

### (i) Ketene

The photochemistry of unsaturated aldehydes might be expected to follow similar mechanistic pathways to the Norrish Type I and II processes observed for saturated carbonyls, producing a pair of radicals or closed shell products (Figure 2). However, this work, and a previous

**Table 4** First order rate coefficients for the loss of ketene intermediates in the dark.

| Unsaturated dicarbonyl | Experiment | $10^3$ *k*(ketene loss) $s^{-1}$ |
|---|---|---|
| (*E*)-2-butenedial | EBUT03 | 2.0 (± 0.4) |
| | EBUT04 | 2.3 (± 0.2) |
| (*Z*)-4-oxo-2-pentenal | ZOXO03 | 4.2 (± 0.3) |
| | ZOXO04 | 4.9 (± 0.2) |
| (*E*)-4-oxo-2-pentenal | EOXO01 | 3.9 (± 0.1) |
| | EOXO02 | 4.0 (± 0.1) |

[a] Reported errors are twice the standard deviation arising from the least squares fit of the data.

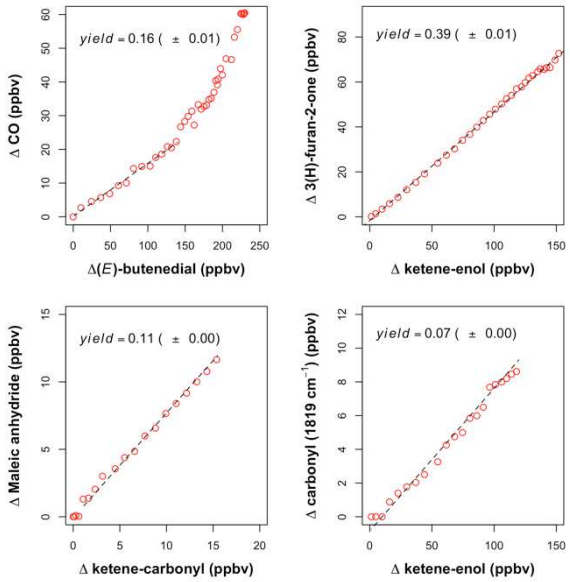


**Figure 8** Yields of primary products with respect to the parent dicarbonyl determined from model fit to measurements for experiment EBUT05.

indoor chamber study of the photochemistry of 2-butenedial and 4-oxo-2-pentenal using arrays of super actinic fluorescent (VIS) and low pressure mercury lamps[19], indicates that the major products are cyclic compounds retaining the carbon backbone of the parent compound. In addition, laboratory flow tube studies of the photolysis of 2-butenedial and 4-oxo-2-pentenal indicate that radical formation channels yielding formyl (HCO) or acetyl ($CH_3CO$) radicals are of negligible importance at wavelengths relevant to the tropospheric boundary layer – 308 and 351 nm[20,21]. These observations suggest that classical Norrish Type I or II processes are not the dominant modes.

The experimental evidence obtained in this work indicates that photo-isomerization to a ketene is the dominant reaction pathway. The ketene appears as a short-lived intermediate which subsequently forms a stable cyclic product, containing the same number of carbon atoms as the initial reactants. The postulated initial step in the formation of the ketene involves the generation of a photoexcited intermediate species, labelled Z* in Figure 4, leading to a biradical, as in the Norrish Type II process. However, rather than fragmentation, this species appears to predominantly rearrange to form a species containing both ketene and enol moieties (Figure 4).

Enols formed from Norrish Type II reactions in laboratory experiments have been observed to tautomerize to carbonyls on a timescale of minutes[25,27,28,42]. It is possible therefore that the measured ketene IR absorption may represent two separate species, a ketene-enol and a ketene-carbonyl. However, it is also possible that the conjugation of the ketene-enol (Figure 4), may increase its stability compared to simpler enols. The tautomerization observed in previous laboratory experiments was reported to likely be driven by heterogeneous chemistry occurring on the reactor walls. Although this process may be assumed to be less efficient in the much larger volume of the EUPHORE chamber, it seems likely to still be a significant process in conversion of the ketene-enol to a ketene-carbonyl.

The dominant fate of the ketene-enol in our experiments is ring-closure to a furanone (an unsaturated lactone) (Figure 9). For (*E*)-2-butenedial, this yields predominantly 2(3*H*)-furanone, with 2(5*H*)-furanone as a minor product (~ 10% of total furanone), for 4-oxo-2-pentenal it yields 5-methyl-2(3*H*)-furanone (5-methyl-2(5*H*)-furanone was not observed). Ring closure of ketene-enols to yield lactones has been observed / inferred in a number of studies previously, particularly in studies of the aromatic compound phthalaldehyde (1,2 benzenedicarbaldehyde). This compound is analogous to (*E*)-2-butenedial, having the unsaturated 1,4 dicarbonyl structure as part of a benzene ring. Phthalide (analogous to the furanone) has been observed as a major product of phthalaldehyde photochemistry both in solution[43-45], and in the gas phase experimentally[46], and theoretically[47]. Pappas and Blackwell[48] originally proposed a mechanism of intramolecular abstraction of the aldehydic hydrogen following photoexcitation to yield a ketene-enol which could undergo ring closure to phthalide. More recently, Fröbel *et al.*[45] monitored the photo-isomerization of o-acetylbenzaldehyde (4-oxo-2-pentenal as part of an aromatic ring) in acetonitrile by femtosecond transient absorption spectroscopy. The authors observed photoexcitation of the parent compound leading to a (*Z*)-ketene-enol apparently formed through two pathways: direct decay of the excited singlet state and a triplet state biradical accessed *via* inter-system crossing.

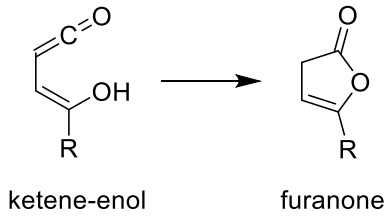


**Figure 9** Formation of the furanone (R = H, 2(3*H*)-furanone; R = $CH_3$, 5-methyl-2(3*H*)-furanone) from ring closure of the ketene-enol.

The formation of the other major cyclic product, maleic anhydride (furan-2,5-dione), appears to be more delayed than the furanone (Figures 6 and 7). Bierbach *et al.*[19] proposed a mechanism for maleic anhydride formation from unsaturated 1,4 dicarbonyl photooxidation involving H removal from one of the aldehyde groups followed by either: (i) direct cyclisation of the alkyl radical; or (ii) via addition of $O_2$, followed by reaction with $NO/HO_2/RO_2$ and subsequent cyclisation of the resultant alkoxy radical. However, neither of these mechanisms is consistent with the delayed onset of formation of maleic anhydride. The observed timing is more consistent with it being a secondary product of the ketene-enol. Formation appears to continue in the dark, apparently ruling out a photolytic mechanism. A tentative pathway for maleic anhydride formation is shown in Figure 10. This involves tautomerization of the enol to a carbonyl, followed by ring closure with elimination of H or $CH_3$ and subsequent reaction with molecular oxygen. However, while this mechanism can fit the observed timing of formation of the product, it requires elimination of a methyl group which might be expected to be have a high energy barrier. Hence we conclude that the formation mechanism of the anhydride remains uncertain. Theoretical studies on these systems are recommended to shed further light on the mechanism.

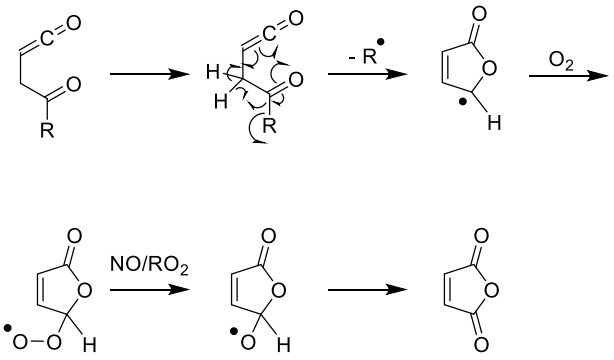


**Figure 10** Postulated mechanism for the formation of maleic anhydride (furan-2,5-dione) from the ketene-carbonyl produced via tautomerization of the ketene-enol.

The formation of unidentified species with absorption features at 1819 $cm^{-1}$ (2-butenedial experiments) and 1829 $cm^{-1}$ (4-oxo-2-pentenal experiments), characteristic of a C=O stretch, was observed in both systems. These species appear to have delayed formation, suggesting that, like the furanone and maleic anhydride, they are also products of the ketene chemistry.

**(ii) Biradical intermediate**

CO is observed as a product in all experiments. In the early part of the experiments, the CO yield with respect to the parent dicarbonyl appears to be linear (Figure 8) suggesting that CO is a primary photolysis product with a yield of ~ 20% from (*E*)-2-butenedial and ~ 10% from 4-oxo-2-pentenal (Table 3). CO is presumed to be formed from molecular elimination of CO from the biradical intermediate (Figure 11). The expected co-products of this pathway are the unsaturated carbonyls acrolein and methyl vinyl ketone, from 2-butenedial and 4-oxo-2-pentenal respectively. These are observed in the respective experiments but are below the limit of quantification.

In the flow tube studies of Tang and Zhu[20] and Xiang *et al.*[21], relatively high yields of acrolein, from 2-butenedial photolysis (yield > 15% at 308 nm, > 23%, 351 nm), and methyl vinyl ketone from 4-oxo-2-pentenal (yield > 40% at 308 nm, > 33%, 351 nm), were measured. As described

above, Fröbel *et al.*[45] suggested that the ketene-enol product detected from photoisomerization of o-acetyl benzaldehyde was formed from both direct decay of the excited singlet state and a triplet state biradical accessed *via* intersystem crossing. If this is the case for the systems studied here, it could explain the larger yields of the unsaturated carbonyls, and lower yields of the furanones, observed in the flow tube studies. These studies were performed at low pressure and in the absence of oxygen – an effective triplet state quencher – meaning that the biradical would be expected to have a longer lifetime and thus have more chance to decay to the unsaturated carbonyl + CO products.

Xiang *et al.*[21] also measured ethane as a product of 4-oxo-2-pentenal photolysis at λ=308 and λ=351 nm, which they interpreted as evidence for a direct elimination channel yielding a methyl radical, with a quantum yield of 31% and 23% at the two wavelengths respectively. Under our experimental conditions, production of the $CH_3$ radical would be expected to produce $CH_3O_2$ which would form HCHO in high yield and, although HCHO is tentatively identified in the FTIR spectra, the upper limit for the yield is only 2%, indicating that this channel is negligible in our experiments.

A possible candidate for the unidentified carbonyls are cyclobutanols formed via Yang cyclisation of the biradical[26]. However, this is in opposition to the observed delayed onset of formation of the species, which suggests formation *via* the ketene rather than the biradical.

**(iii) Summary**

The overall mechanism proposed for unsaturated 1,4-dicarbonyl photolysis based on the results presented herein is shown in Figure 11. To summarise, the parent compound is excited to a photoexcited complex (*Z**) and then, following H atom transfer, either isomerises to a ketene-enol or a biradical species. This biradical can either eliminate CO to yield an unsaturated carbonyl or form the ketene-enol species. The ketene-enol can subsequently undergo ring closure to a furanone, or tautomerize to a ketene-carbonyl. This species can undergo ring closure to maleic anhydride. The products from this scheme (Table 3) account for about 75% of the loss of the parent compound for (*E*)-2-butenedial and 55% for 4-oxo-2-pentenal. Including the unidentified carbonyl increases this to ~ 90% and 70 % respectively.

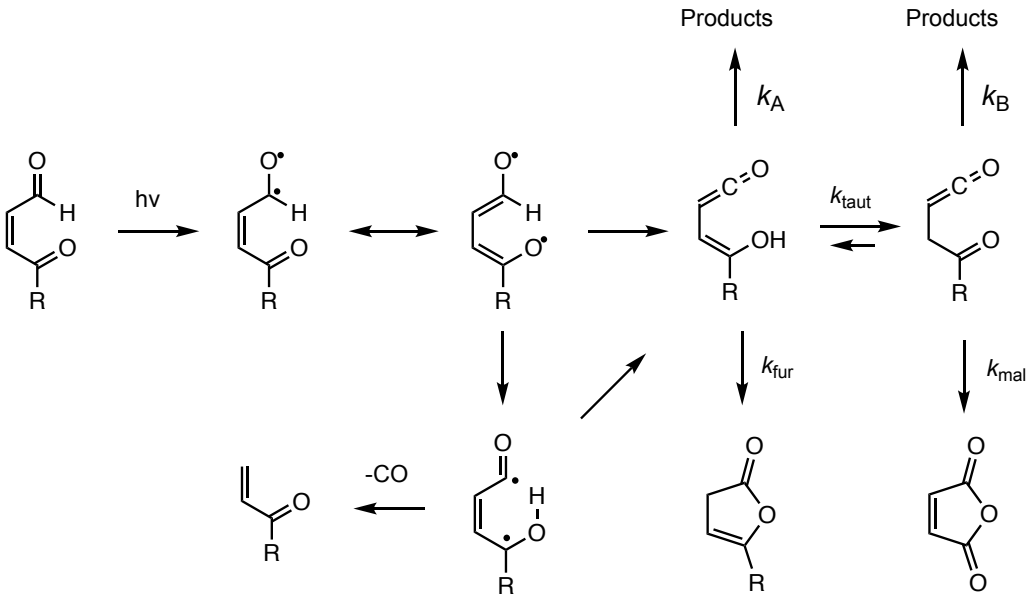


**Figure 11** Proposed overall photochemical mechanism for unsaturated 1,4-dicarbonyls (R= H for 2-butenedial, R= $CH_3$ for 4-oxo-2-pentenal).

**Mechanism Simulations**

A simple model was developed to represent the chemical mechanism shown in Figure 11. The results of model simulations using the initial conditions of the EBUT05 and ZOXO05 experiments and the proposed mechanism, with values constrained to give a best fit, are shown in Figure 12.

The measured ketene species is assumed to represent both a ketene-enol (KETA) and a ketene-carbonyl (KETB) species. Three possible losses are considered for KETA: ring closure to the furanone (FUR) $k_{fur}$, tautomerization to KETB, $k_{taut}$, and another route representing any additional loss processes, $k_A$. For KETB two losses are considered: ring closure to maleic anhydride (MAL), $k_{mal}$, and a route representing any other loss processes, $k_B$. CO is produced only as a primary photolysis product, with a yield of 0.2 from 2-butenedial and 0.1 from 4-oxo-2-pentenal.

The photochemical loss rate of the parent dicarbonyl is constrained by fitting to the measurements (Figure 12 – insets). The total loss rate of KETA is constrained by fitting to the measured ketene profile. $k_{fur}$ is constrained by assigning to it a portion of the total loss of KETA and fitting to the measured furanone mixing ratios (for butenedial it is fitted to the measured mixing ratios of 2(3*H*)-furanone divided by 0.9, as production of the isomer

**Table 5** Reactions and kinetic parameters used in the model profile fits

| Reactant | Products | Reaction | Rate $10^3$ $s^{-1}$ |
|---|---|---|---|
| **(*E*)-2-butenedial** | 0.8*KETA + 0.2*CO | hν | [a] |
| KETA | 0.9* FUR | $k_{fur}$ | 2.9 (± 0.5) |
| | KETB | $k_{taut}$ | 0.9 (± 0.05) |
| | OTHER | $k_A$ | 1.4 (± 0.4) |
| KETB | MAL | $k_{mal}$ | 2.6 (± 1.0) |
| | | $k_B$ | - [b] |
| **(*Z*)-4-oxo-2-pentenal** | 0.9*KETA' + 0.1*CO | hν | [a] |
| KETA' | FUR' | $k_{fur}$' | 2.7 (± 0.3) |
| | KETB' | $k_{taut}$' | 2.4 (± 0.3) |
| | OTHER | $k_A$' | 1.6 (± 0.5) |
| KETB' | MAL | $k_{mal}$' | 0.9 (± 0.2) |
| | | $k_B$' | 6.0 (± 0.0) |

[a] Rate constrained by measured loss of parent compound

[b] No sink required to fit the data.

2(5*H*)-furanone was observed to be ~ 10% of 2(3*H*)-furanone).

Loss rates for the furanones to OH were included using $k$(2(3*H*)-furanone+OH) = 4.45 × $10^{-11}$ $cm^3$ $s^{-1}$ and $k$(5-methyl-2(3*H*)-furanone+OH) = 6.9 × $10^{-11}$ $cm^3$ $s^{-1}$ [19]. Assuming [OH] = 8 × $10^5$ $cm^{-3}$ gives a good agreement with the observed furanone mixing ratios.

The value for ($k_A$ + $k_{taut}$), which combined with $k_{fur}$ gives the total loss rate of KETA, is constrained by fitting to the measured ketene profile. The values for $k_{taut}$ and $k_{mal}$ are then constrained by fitting to the measured mixing ratios of maleic anhydride.

Reaction rates derived for the 2-butenedial (EBUT01, 02, 04 and 05) and 4-oxo-2-pentenal (ZOXO01, 02, 04 and 05; EOXO01 and 02) systems from the model simulations are shown in Table 5. Uncertainties represent the spread in model derived values across the different experiments.

The values for $k_{fur}$, the rate of ring closure of the enol to the furanone, are similar for the two systems, 2.5 – 3 × $10^{-3}$ $s^{-1}$. Likewise, the additional loss process, $k_A$, required to fit the measurements is also of a similar rate for the two systems ~ 1.5 × $10^{-3}$ $s^{-1}$. The rate of enol tautomerism to the carbonyl, $k_{taut.}$, appears to be significantly faster in the 4-oxo-2-pentenal system (2.4 × $10^{-3}$ $s^{-1}$ compared to 0.9 × $10^{-3}$ $s^{-1}$ for 2-butenedial). Shaw *et al.*[28] showed that tautomerization of isomeric enol species can occur at quite different rates, with 2-propenol converting to acetone significantly faster than 1-propenol converting to propanal. Similarly, in this work. the enol converts faster to the ketone than to the aldehyde. The conversion of the carbonyl to maleic anhydride is significantly faster in the (*E*)-2-butenedial system. A large additional sink of the carbonyl in the 4-oxo-2-pentenal system, $k_B$, is also required to simulate the observed maleic anhydride mixing ratios.

## Atmospheric Implications

The mean rate coefficients ($j$ values) for photochemical loss of the unsaturated dicarbonyls are used to calculate the tropospheric lifetimes of the compounds assuming a value of $j(NO_2)$ = 8 × $10^{-3}$ $s^{-1}$, a typical value for solar noon during summer months[49]. The atmospheric lifetimes due to reaction with OH, $NO_3$ and $O_3$ have also been determined using reported rates in the literature. The resulting lifetimes, presented in Table 6, indicate that all isomers of 2-butenedial and 4-oxo-2-pentenal are removed photochemically very quickly, with lifetimes on the order of 10 - 15 minutes.

The atmospheric lifetimes due to reaction with OH radicals are 180 - 200 minutes, whilst the lifetimes for the $O_3$ and $NO_3$ reactions are of the order of days. Thus photochemical loss is clearly the major atmospheric fate of the unsaturated dicarbonyls in the boundary layer, with a minor contribution (up to 5%) from the reaction with OH radicals.

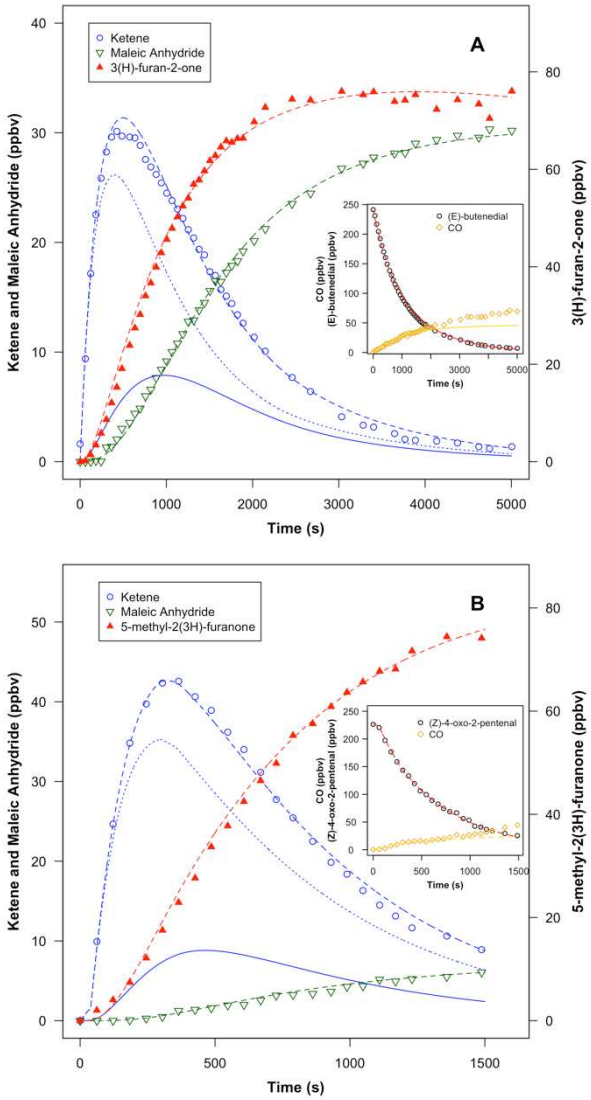


**Figure 12** Model simulation fits to measurements from EBUT05 (**A**) and ZOXO05 (**B**). Lines are modeled mixing ratio profiles. Blue dashed line – total ketene (i.e. KETA + KETB); blue dotted line – KETA; blue solid line – KETB.

**Table 6** Rate coefficients and corresponding lifetimes for the atmospheric loss processes of 2-butenedial and 4-oxo-2-pentenal

| Compound | $k$(OH) $10^{-11}$ cm$^3$ s$^{-1}$ | $\tau$(OH) [c] Hours | $k$($O_3$) $10^{-18}$ cm$^3$ s$^{-1}$ | $\tau$($O_3$) [d] Days | $k$($NO_3$) $10^{-14}$ cm$^3$ s$^{-1}$ | $\tau$($NO_3$) [e] Days | $j$(dicarb.)/$j$($NO_2$) | $\tau$(photolysis) [g] Minutes |
|---|---|---|---|---|---|---|---|---|
| 2-butenedial [a] | | | 1.6 (± 0.1) | 10.5 | | | | |
| (*Z*)-2-butenedial | 5.2 (± 0.1) | 3.4 | 2 [b] | 8.3 | 1 [b] | 2.3 | 0.18 [f] | 11 |
| (*E*)-2-butenedial | ≥ 2.4 (± 0.8) | ≤ 7.1 | 2 [b] | 8.3 | 1 [b] | 2.3 | 0.14 | 15 |
| 4-oxo-2-pentenal [a] | 5.6 (± 0.2) | 3.1 | 4.8 (± 0.8) | 3.4 | 1 [b] | 2.3 | | |
| (*Z*)-4-oxo-2-pentenal | | | | | | | 0.21 | 10 |
| (*E*)-4-oxo-2-pentenal | | | | | | | 0.18 | 11 |

[a] Mixture of *E* and *Z* isomers; [b] Estimation based on structure activity relationships; [c] Assuming daily mean [OH] = $1.6 \times 10^6$ cm$^{-3}$ ; [d] Assuming daily mean [$O_3$] = $4 \times 10^{11}$ cm$^{-3}$ ; [e] Lifetime at night assuming mean [$NO_3$] = $5 \times 10^8$ cm$^{-3}$ ; [f] Sorensen and Barnes[37] ; [g] Assuming $j(NO_2) = 8 \times 10^{-3}$ s$^{-1}$

From the experiments reported here, the photochemistry of unsaturated 1,4-dicarbonyls would be expected to yield cyclic furanone species as the major products. However, in the boundary layer, photolytic processes or reaction of OH with the ketene or enol moieties may also be important. There is little known about the subsequent atmospheric degradation of the furanones under boundary layer conditions, however, they are expected to react over a timescale of hours[19], and are thus likely to contribute to regional ozone formation and secondary organic aerosol production[6,50-52].

The extent of radical production from the photolysis of 2-butenedial and 4-oxo-2-pentenal also needs to be considered because species such as $HO_2$ play a major role in determining the oxidizing capacity of the atmosphere. The principal radical producing channel during the photolysis of aldehydes is the Norrish Type I process. However, this channel is negligible for 2-butenedial and 4-oxo-2-pentenal, where the most likely radical-producing channel is the formation of maleic anhydride, which produces two molecules of $HO_2$ (or $CH_3O_2$ + $HO_2$) based on the proposed mechanism. Based on the yields determined for maleic anhydride, it is estimated that, in the absence of NO, the yields of $HO_2$ produced during the photolysis of 2-butenedial and 4-oxo-2-pentenal are < 20% and < 5% respectively.

## Conclusions

The photochemical loss rates of the unsaturated 1,4-dicarbonyls, *(E)*-2-butenedial, *(E)*-4-oxo-2-pentenal, and *(Z)*-4-oxo-2-pentenal, relative to $j(NO_2)$, have been determined to be 0.14 (±0.02), 0.18 (±0.01), and 0.20 (±0.03) respectively under ambient light conditions in the EUPHORE large outdoor simulation chamber. At these rates, photochemical loss is expected to be the dominant fate of these compounds under boundary layer conditions. The photochemical mechanism appears to proceed via γ-H abstraction followed by isomerisation to a ketene-enol species. A minor channel is decomposition of a biradical intermediate species to yield an unsaturated carbonyl and CO. Isomerisation of the ketene-enol species leads to the major observed product, a furanone. The ketene-enol species can also tautomerise to a ketene-carbonyl, before undergoing cyclisation to give maleic anhydride (furan-2,5-dione), which is also observed in significant yield. Radical forming channels are minor, suggesting that the initial photochemical reactions should have little contribution to ozone production. However, subsequent oxidation pathways and products of the major furanone and furandione products, are yet to be fully elucidated.

## Acknowledgements

The experiments were carried out during two measurement campaigns as part of the EU research project EXACT (Effects of the oxidation of aromatic compounds in the troposphere, contract no. EVK2-CT-1999-00053). The excellent technical support provided by Dr Klaus Wirtz and colleagues at the EUPHORE facility during these campaigns is gratefully acknowledged. This work has received funding from the European Union's Horizon 2020 research and innovation programme through the EUROCHAMP-2020 Infrastructure Activity under grant agreement No 730997. Mike Newland and Andrew Rickard also acknowledge support from the Mechanisms for Atmospheric chemistry: GeneratioN, Interpretation and FidelitY – MAGNIFY project, funded by the UK Natural Environment Research Council (NERC, via grant NE/M013448/1).

## REFERENCES

1 E. Gómez Alvarez, J. Viidanoja, A. Muñoz, K. Wirtz and J. Hjorth, *Environ. Sci. Technol*., 2007, **41**, 8362-8369.

2 E. Gómez Alvarez, E. Borrás, J. Viidanoja, and J. Hjorth, *Atmos. Environ*., 2009, **43**, 1603-1612.

3 S. M. Aschmann, N. Nishino, J. Arey and R. Atkinson, *J. Phys. Chem. A*, 2014, **118**, 457-466.

4 Y. Yuan, X. Zhao, S. Wang and L. Wang, *J. Phys. Chem. A*, 2017, **121**, 9306-9319.

5 Y. Qian, L. Zhu, Y. Wang and X. Lu, *Renewable and Sustainable Energy Reviews*, 2015, **41**, 633–646.

6 C. Bloss, V. Wagner, A. Bonzanini, M. E. Jenkin, K. Wirtz, M. Martin-Reviejo and M. J. Pilling, *Atmos. Chem. Phys*., 2005, **5**, 623-639.

7 L. Wang, R. Wu and C. Xu, *J. Phys. Chem. A*, 2013, **117**, 14163-14168, 2013.

8 R. Wu, S. Pan, Y. Li and L. Wang, *J. Phys. Chem. A*, 2014, **118**, 4533-4547.

9 S. Pan and L. Wang, *J. Phys. Chem. A*, 2014, **118**, 10778-10787.

10 Y. Ji, J. Zhao, H. Terazono, K. Misawa, N. P. Levitt, Y. Li, Y. Lin, J. Peng, Y. Wang, L. Duan, B. Pan, F. Zhang, X. Feng, T. An, W. Marrero-Ortiz, J. Secrest, A. L. Zhang, K. Shibuya, M. Molina and R. Zhang, *Proc. Natl. Acad. Sci. USA*, 2017, **114**, 8169–8174.

11 M. J. Newland, M. E. Jenkin and A. R. Rickard, *Proc. Natl. Acad. Sci. USA*, 2017, **114**, doi: 10.1073/pnas.1713678114.

12 T. Berndt and O. Böge, *Phys. Chem. Chem. Phys*., 2006, **8**, 1205-1214.
13 D. F. Smith, C. D. McIver and T. E. Kleindienst, *J. Atmos. Chem*., 1998, **30**, 209-228.
14 J. Arey, G. Obermeyer, S. M. Aschmann, S. Chattopadhyay R. D. Cusick and R. Atkinson, *Environ. Sci. Technol*., 2009, **43**, 683-689.
15 A. W. Birdsall, J. F. Andreoni and M. J. Elrod, *J. Phys. Chem. A*, 2010, **114**, 10655-10663.
16 D. F. Smith, C. D. McIver and T. E. Kleindienst, *J. Atmos. Chem*., 1999, **34**, 339-364.
17 J. F. Hamilton, A. C. Lewis, C. Bloss, V. A. Wagner, P. Henderson, B. T. Golding, K. Wirtz, M. Martin-Reviejo, and M. J. Pilling, *Atmos. Chem. Phys*., 2003, **3**, 1999-2014.
18 J. Yu, H. E. Jeffries and K. G. Sexton, *Atmos. Environ*., 1997, **31**, 2261-2280.
19 A. Bierbach, I. Barnes, K. H. Becker and E. Wiesen, *Environ. Sci. Technol*., 1994, **28**, 715-729.
20 Y. Tang and L. Zhu, *Chem. Phys. Letts*., 2005, **409**, 151-156.
21 B. Xiang, L. Zhu and Y. Tang, *J. Phys. Chem. A*, 2007, **111**, 9025-9033, 2007.
22 X. Liu, H. E. Jeffries and K. G. Sexton, *Environ. Sci. Technol*., 1999, **33**, 4212-4220.
23 J. G. Calvert, A. Mellouki, J. J. Orlando, M. J. Pilling and T. J. Wallington, The Mechanisms of Atmospheric Oxidation of the Oxygenates, Oxford University Press, 2011.
24 J. Tadić, I. Juranić and G. K. Moortgat, *J. Photochem. Photobiol. A*, 2001a, **143**, 169-179.
25 J. M. Tadić, I. O. Juranić and G. K. Moortgat, *J. Chem. Soc. Perkin Trans. 2*, 2002, **2**, 135-140.
26 N. C. Yang and D. D. H. Yang, *J. Am. Chem. Soc*., 1958, **80**, 2913-2914.
27 G. R. McMillan, J. G. Calvert and J. N. Pitts Jr, *J. Am. Chem. Soc*., 1964, **86**, 3602-3605.
28 M. F. Shaw, D. L. Osborn, M. J. T. Jordan and S. H. Kable, *J. Phys. Chem. A*, 2017, **121**, 3679-3688.
29 J. W. Coomber, J. N. Pitts Jr. and R. R. Schrock, *Chem. Commun.,* **0**, 1968, 190-191.
30 M. P. O'Connor, J. C. Wenger, A. Mellouki, K. Wirtz and A. Muñoz, *Phys. Chem. Chem. Phys*., 2006, **8**, 5236-5246.
31 M. E. Jenkin, S. M. Saunders and M. J. Pilling, *Atmos. Environ*., 1997, **31**, 81–104.
32 K. H. Becker, EUPHORE: Final Report to the European Commission, Contract EV5V-CT92-0059, Bergische Universität, Wuppertal, Germany, 1996.
33 B. Klotz, S. Sørensen, I. Barnes, K. H. Becker, T. Etzkorn, R. Volkamer, U. Platt, K. Wirtz and M. Martin-Reviejo, *J. Phys. Chem. A*, 1998, **102**, 10289-10299.
34 W. B. DeMore, S. P. Sander, C. J. Howard, A. R. Ravishankara, D. M. Golden, C. E. Kolb, R. F. Hampson, M. J. Kurylo and M. J. Molina, in Chemical kinetics and photochemical data for use in stratospheric modelling, Evaluation number 12, JPL Publ. 97-4, 266, 1997.
35 W. J. Bloss, J. D. Lee, C. Bloss, D. E. Heard, M. J. Pilling, K. Wirtz, M. Martin-Reviejo and M. Siese, *Atmos. Chem. Phys*., 2004, **4**, 571−583.
36 M. Siese, K. H. Becker, K. J. Brockmann, H. Geiger, A. Hofzumahaus, F. Holland, D. Mihelcic and K. Wirtz, *Environ. Sci. Technol*., 2001, **35**, 4660-4667.
37 S. Sørensen and I. Barnes, Photolysis of unsaturated 1,4 dicarbonyls, in EUPHORE Report 1997, Ed. Barnes, I.; Wenger, J., Department of Physical Chemistry, Bergische Universität Wuppertal, Wuppertal, Germany, 1998.
38 G. K. Moortgat, Final report on EU project RADICAL: "Evaluation of radical sources in atmospheric chemistry through chamber and laboratory studies", 2000.
39 G. K. Moortgat, Important photochemical processes in the Atmosphere, *Pure and Applied Chemistry*, 2001, **73**, 487.
40 B. Klotz, I. Barnes and K. H. Becker, *Int. J. Chem. Kinet*., 1999, **31**, 689-697.
41 T. T. Tidwell, Ketenes II, Section 5.4.4. p520-525, John Wiley & Sons Inc., Hoboken, New Jersey, USA, 2006.
42 J. Tadić, I. Juranić and G. K. Moortgat, *Molecules*, 2001b, **6**, 287-299.
43 J. Kagan, *Tetrahedron Lett*., 1966, **7**, 6097-6102.
44 L. Plíštil, T. Šolomek, J. Wirz, D. Heger and P. Klán, *J. Org. Chem*., 2006, **71**, 8050-8058.
45 S. Fröbel, L. Buschhaus, T. Villnow, O Weingart and P. Gilch, *Phys. Chem. Chem. Phys*., 2015, **17**, 376-386.
46 Y. Chen, PhD Thesis, University College Cork, 2012.
47 Q. Li, A. Migani and L. Blancafort, *Phys. Chem. Chem. Phys*., 2012, **14**, 6561-6568.
48 S. P. Pappas and J. E. Blackwell Jr, *Tetrahedron Lett*., 1968, **9**, 3337-3340.
49 D. D. Parrish, P. C. Murphy, D. L. Albritton and F. C. Fehsenfled, *Atmos. Environ*., 1983, **17**, 1365-1379.
50 D. Johnson, M. E. Jenkin, K. Wirtz and M. Martin-Reviejo, M., *Environ. Chem*., 2004, **1**, 150-165.
51 D. Johnson, M. E. Jenkin, K. Wirtz and M. Martin-Reviejo, *Environ. Chem*., 2005, **2**, 35-48.
52 A. R. Rickard, K. P. Wyche, A. Metzger, P. S. Monks, A. M. Ellis, J. Dommen, U. Baltensperger, M. E. Jenkin and M. J. Pilling, *Atmos. Environ*., 2010, **44**, 5423-5433.